Available online at www.sciencedirect.com
ScienceDirect
Catalysis Today 128 (2007) 129–137
CATALYSIS TODAY
www.elsevier.com/locate/cattod

Nanosize cobalt oxide-containing catalysts obtained through microwave-assisted methods

M. Herrero, P. Benito, F.M. Labajos, V. Rives *

Departamento de Química Inorgánica, Universidad de Salamanca, Salamanca 37008, Spain

Available online 15 August 2007

Abstract

Nanosized cobalt mixed oxide, with high stability of Co(II), were obtained by controlled thermal decomposition of layered double hydroxides (LDHs) with Co, Zn and Al in the brucite-type sheets. The effect of the microwave ageing treatment of the LDHs into the properties of the calcined products was studied. For this reason, the precursors were submitted to increasing periods of time to microwave-hydrothermal treatment. The use of microwave ageing yields to well-crystallised compounds without oxidation of Co^{2+} species to Co^{3+}. The structure features of oxides remain during whole ageing process; the microwave-hydrothermal treatment yield, in all cases, spinel-like compounds. Studies of surface properties, N_2 adsorption/desorption and the TEM micrographs, show that the textural properties are strongly modified depending on the irradiation time were submitted to, altering both the pore size distribution and the particle size of the nano-oxides.

Keywords: Hydrotalcite; Microwave; Mixed oxides

1. Introduction

The cobalt spinel compounds (including $ZnCo_2O_4$) can act as efficient catalysts in a number of heterogeneous chemical processes, such as CO oxidation [1], catalytic combustion of hydrocarbons [2] or selective oxidation and reduction of several organic molecules [3]. The most general method for preparing oxide spinels involves solid-state reaction of the parent metal oxides which are mechanically mixed in the form of finely divided powders. However, for attaining complete reaction, a temperature of about 1000 °C (or higher) has to be maintained for several days [4]. The disadvantages of solid-state routes, such as inhomogeneity, lack of stoichiometry control, and larger particle size, can be avoided when the material is obtained through the thermal treatment of layered double hydroxides, and the textural properties improved using microwave heating.

Layered double hydroxides (LDHs), also known as anionic clays or hydrotalcite-like compounds, are an important class of materials whose structure can be described as brucite-like layers, $Mg(OH)_2$, where some of the divalent cations have been replaced by trivalent ones, giving rise to positively charged sheets; electrical neutrality is maintained by means of anions located in the interlayer region, where water molecules are also found [5,6]. These compounds are represented by the general formula $[M_{1-x}^{2+}M_x^{3+}(OH)_2]^{x+}[(A^{n-})_{x/n}\cdot mH_2O]^{x-}$; and A^{n-} is a charge-balancing anion, such as CO_3^{2-}, NO_3^-, Cl^-, etc. LDHs containing more that one M^{2+} cation and/or more that one M^{3+} cation in the layers have been also reported [7–9].

An interesting aspect of LDHs chemistry is their use as catalysts after a controlled thermal treatment, generally around 450–550 °C [10]. At these temperature LDHs loose their layered structure and form mixed metal oxides with high thermal stability, high surface area, high and homogeneous dispersion of metal cations and small crystal size. In addition, transition metal cations present in the brucite-like layers of LDHs can be precursors of redox- and Lewis-type centres, showing outstanding catalytic activity. The efficiency of the material depends on its microstructural properties, which are sensitive to the preparation method [11], thereof playing a very important role with regard to the chemical, structural, and magnetic properties of the mixed oxides [12]. Thus it seems to be essential to prepare well-crystallised LDH of high purity to avoid a segregation of the components.

* Corresponding author. Tel.: +34 923294489; fax: +34 923294574.
E-mail address: vrives@usal.es (V. Rives).

0920-5861/$ – see front matter © 2007 Elsevier B.V. All rights reserved.
doi:10.1016/j.cattod.2007.06.070

Microwave radiation (hereafter MW) under hydrothermal conditions has been recently applied for the rapid crystallization of LDHs [13,14]. It has been reported that hydrotalcites prepared by this method are constituted by smaller crystallites with higher specific surface areas than those for samples prepared by conventional methods, and probably this preparation procedure induces higher amounts of surface-defective sites [15]. Recently, we have reported the use of microwave irradiation to prepare well-crystallised LDH materials, where oxidation of Co(II) species to Co(III) ones during the preparation procedure was avoided [16]. In addition, this method leads to solids with homogeneous particle size, and, even more important, the time required to prepare the samples is much shorter and thus energy saving is also important [17]. These improvements are a consequence of the rapid and homogeneous heating of the material upon its exposure to the microwave radiation.

In this paper we report the preparation of layered double hydroxides with Co, Zn and Al in the brucite-type sheets, as precursors of Co, Zn, Al-mixed oxides. In order to optimise the properties of the mixed oxides different ageing treatments of the LDHs have been tested, i.e., the initial slurry obtained by coprecipitation of the metal cation hydroxides was aged for different periods of time under the influence of the MW radiation at 100 °C, and then the solids were calcined at 550 °C to prepare the mixed oxides.

2. Experimental

2.1. Preparation of the solids

The samples were prepared by the coprecipitation method described by Reichle [18]. The chemicals, $Co(NO_3)_2{\cdot}6H_2O$, $Zn(NO_3)_2{\cdot}6H_2O$, $Al(NO_3)_3{\cdot}9H_2O$, NaOH, and Na_2CO_3 were from Fluka. The nominal (Co + Zn)/Al and Co/Zn molar ratios were 2/1 and 1/1, respectively. The pH of the synthesis was kept at a constant value of 9 by dropwise addition of a 1 M NaOH solution from a pH-burette 240 from Crison. The slurry obtained was submitted to MW-hydrothermal treatment for different periods of time (10, 30, 60, 180 or 300 min) at 100 °C. The MW-hydrothermal experiments were carried out in a Milestone Ethos Plus MW oven where reactants were treated in Teflon liners. The microwave oven uses a 2.45 GHz frequency radiation and the power supplied was that necessary to attain the temperature previously programmed, which was measured by a thermocouple. The precipitates were separated and washed by centrifugation with distilled water until complete removal of counterions and dried at 40 °C in a furnace at open air.

The samples were labelled depending on the hydrothermal treatment time at which they were been submitted, CZA0 for the fresh sample, i.e. not aged, CZA*t* for the samples submitted to MW-hydrothermal method, where *t* stands for the irradiation time in min.

Calcination of the samples was carried out at 550 °C, in flowing air at a heating rate of 10 °C min^{-1}. The final temperature was maintained for 2 h.

2.2. Characterisation techniques

Element chemical analyses for Co, Zn and Al were carried out by atomic absorption in a Mark 2 ELL-240 apparatus. Powder X-ray diffraction (PXRD) patterns were recorded in a Siemens D-500 instrument using Cu Kα radiation (λ = 1.54050 Å) and equipped with Diffract AT software. Identification of the crystalline phases was made by comparison with the JCPDS files [19]. UV–vis spectra were recorded following the diffuse reflectance (UV–vis/DR) technique in a Perkin-Elmer Lambda 35 instrument with a Labsphere RSA-PE-20 integrating sphere and software UV WinLab, using 2 nm slits and MgO as reference. Thermogravimetric (TG) and differential thermal analyses (DTA) were carried out in TG-7 and DTA-7 instruments from Perkin-Elmer, in flowing oxygen and/or nitrogen, at a heating rate of 10 °C min^{-1}. FT-IR spectra were recorded in a Perkin-Elmer FT1730 instrument, using KBr pellets; 100 spectra (recorded with a nominal resolution of 4 cm^{-1}) were averaged to improve the signal-to-noise ratio. Temperature-programmed reduction (TPR) analysis was carried out in a Micromeritics 2900 TPD/TPR instrument. The reducing agent was H_2/Ar (5 vol.%) and the gas flow (50 ml min^{-1}), sample weight (15–20 mg), and heating schedule (10 °C min^{-1}) were chosen according to the literature [20] to optimize resolution of the curves. Calibration of the instrument was carried out with CuO (from Merck). Specific surface assessment was carried out in a Gemini instrument from Micromeritics. The sample (ca. 80–100 mg) was previously degassed in flowing nitrogen at 110 °C for 2 h in a FlowPrep 060 apparatus, also from Micromeritics, in order to remove physisorbed water, and the data were analysed using published software [21]. Transmission electron microscopy (TEM) was performed using a Zeiss 902. The TEM samples were ultrasonically dispersed in acetone and then a suspension was deposited onto holey carbon film deposited on a Cu grid.

Table 1
Co/Zn and (Co + Zn)/Al molar ratio formula of the solids, lattice parameters (*c*, *a*, in Å) and average particle size from X-ray diffraction lines broadening (*D*, in Å)

Sample	Co/Zn[a]	(Co + Zn)/Al[a]	Formulae	*c*	*a*	*D*
CZA0	1.04	2.34	$[Co_{0.36}Zn_{0.34}Al_{0.30}(OH)_2]\ (CO_3)_{0.15}{\cdot}0.97H_2O$	22.95	3.066	120
CZA10	1.04	2.37	$[Co_{0.36}Zn_{0.34}Al_{0.30}(OH)_2]\ (CO_3)_{0.15}{\cdot}1.00H_2O$	22.55	3.062	140
CZA30	1.06	2.38	$[Co_{0.36}Zn_{0.34}Al_{0.30}(OH)_2]\ (CO_3)_{0.15}{\cdot}0.93H_2O$	22.73	3.068	140
CZA60	1.04	2.27	$[Co_{0.35}Zn_{0.34}Al_{0.31}(OH)_2]\ (CO_3)_{0.16}{\cdot}0.96H_2O$	22.73	3.066	160
CZA180	1.02	2.28	$[Co_{0.35}Zn_{0.34}Al_{0.31}(OH)_2]\ (CO_3)_{0.16}{\cdot}0.93H_2O$	22.69	3.068	180
CZA300	1.05	2.35	$[Co_{0.36}Zn_{0.34}Al_{0.30}(OH)_2]\ (CO_3)_{0.15}{\cdot}1.00H_2O$	22.67	3.068	150

[a] Molar ratio.

3. Results

3.1. Characterisation of the precursors

Table 1 displays details of the chemical composition of the samples prepared. The carbonate content was calculated from the M^{2+}/Al^{3+} atomic ratios, assuming carbonate is the only charge-balancing interlayer anion, and the oxidation state of Co^{2+} is unaffected during the synthesis procedure, in agreement with other experimental results (see below). The interlayer water content was determined from the TG curves. In all cases, the M^{2+}/M^{3+} ratios are somewhat higher than the expected ones. The small deviation observed is rather common [10] and has been usually ascribed to a preferential precipitation of one or another cation as hydroxide [22]. On the other hand, the Co/Zn ratios in the solids were reasonably coincident with the ratios in the starting solutions. When looking at these values for the samples submitted to the MW radiation for different periods of time, it can concluded that prolonging the irradiation time has no major effect on the chemical composition, as the changes in the Co/Zn are lower than 3% and the M^{2+}/M^{3+} ratios change randomly within a very narrow range (less than 5%), i.e., the LDH structure is stable under the preparation conditions here used.

The PXRD patterns of the layered precursors are shown in Fig. 1a. They show the presence of pure and well-crystallised hydrotalcite-like phases for all samples, without co-crystallization of any detectable impurity. A steady enhancement in the crystalline degree of the solids (as qualitatively measured from the sharpness of the diffraction maxima, especially the first one recorded at a low diffraction angle) is attained as the irradiation time is increased. The ordering is achieved both in the stacking direction, as the (0 0 3), (0 0 6) and (0 0 9) diffraction lines become sharper and more intense as the irradiation time is increased, as well as within the layers, as the doublet corresponding to planes (1 1 0) and (1 1 3) ($2\theta = 60$–65°) is better resolved for the long time-treated samples.

The cell parameters have been calculated assuming a 3R polytype [23]. Lattice parameter c was calculated from the position of the first basal peak as $c = 3d_{(0\,0\,3)}$, while the a values were calculated from the (1 1 0) reflection close to $2\theta = 60$–65°, according to the equation $a = 2d_{(1\,1\,0)}$. The crystallite sizes were determined by the Debye–Scherrer equation from the full width at half-maximum (FWHM) intensity of the (0 0 3) diffraction peak for each sample. The Warren correction was used for instrumental line broadening, while the possible contribution of the disorder effect and/or lattice strains was ignored [24]. The calculated values for all these three parameters are included in Table 1. The c values are quite similar for all the samples, although the value for the fresh, untreated sample (CZA0), is slightly larger than for the MW-treated samples. The a values remain almost constant in all cases, and the differences found can be within experimental error. The value of parameter a corresponds to the shortest average distance between cations in the close-packed sheets and it can be correlated to the average radii of the metal cations in the layers, as it depends on the chemical composition of the layers. The observed improvement in the crystallinity degree as

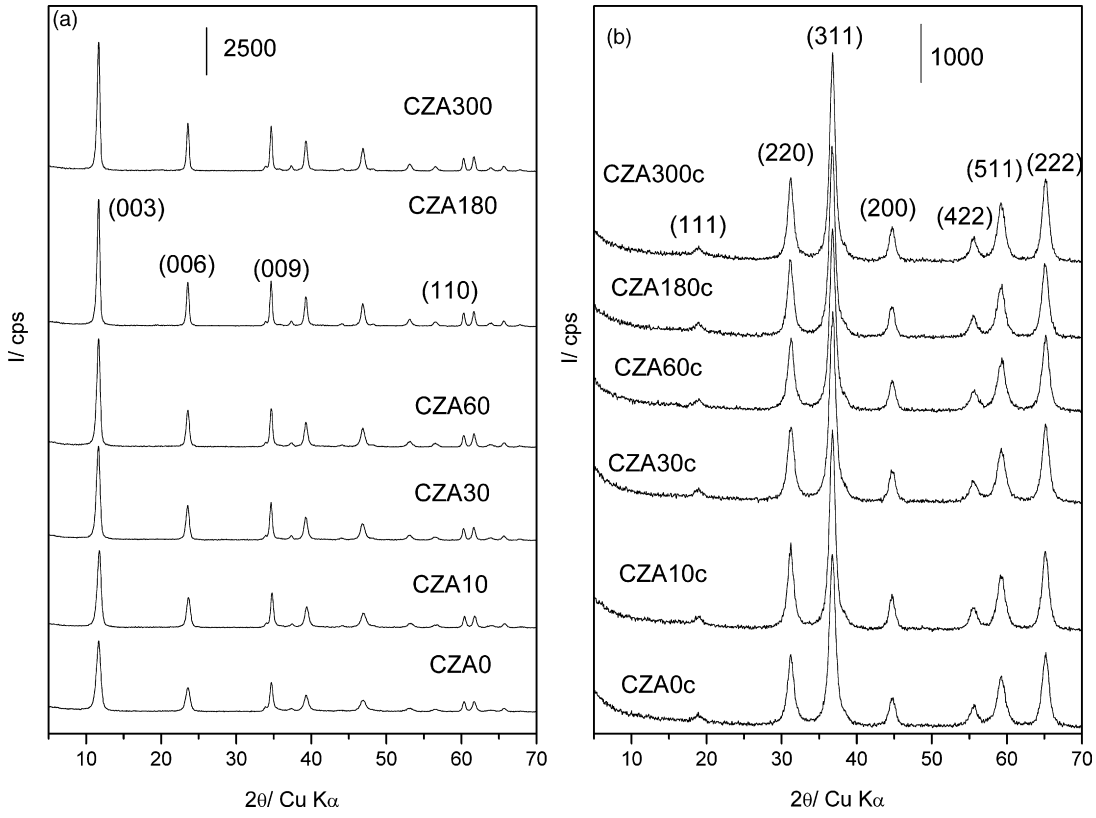

Fig. 1. Powder X-ray diffraction patterns of (a) the layered precursors and (b) the calcined solids. The patterns have been vertically displaced for clarity.

the duration of the MW treatment is increased correlates with an increase in the average crystallite size. The maximum crystallite size is achieved after 180 min treatment, while a further increase of the ageing time leads to a decrease of the crystallinity degree (smaller crystallite size).

The FT-IR spectra also give some clues about the order enhancement [25]. The FT-IR spectra show the characteristic bands for hydrotalcite-like compounds [26,27]; however, some modifications of the bands are observed along the MW treatment. By increasing the irradiation time, the shoulder due to the ν_{OH} stretching mode of hydroxyl groups bonded to carbonate anions in the interlayer, recorded usually around 2900 cm^{-1}, becomes more remarkable. In addition, the ν_3 mode of the carbonate species becomes more symmetric and the bands recorded in the low wavenumbers region are better resolved. These results indicate that the microwave treatment does not only gives rise to a better ordering of the hydroxide layers, but also to an ordering of species in the interlayer region.

The vis–UV spectra of all the samples are characteristic of Co-hydrotalcites in which all the divalent cobalt cations are located in an octahedral environment [28]. In this case it seems that the simultaneous presence of a third cation, zinc, in the layer composition and/or the precise nature of the ageing treatment given (hydrothermal treatment under MW irradiation) decreases the easiness with which the $Co^{2+} \rightarrow Co^{3+}$ oxidation process takes place.

In order to check the approximate average oxidation state of the cobalt cations, the TPR profiles of the samples have been recorded. The curves are rather similar for all samples. In some cases a very weak reduction process can be recorded with a maximum reduction rate close to 345 °C, which can be ascribed to early reduction of some remaining nitrates [29], although no clear detection of this species can be concluded from the FT-IR spectra. The main reduction process takes place between 450 and 725 °C. Two overlapped peaks are recorded in this range for all samples, with an absolute maximum at ca. 660 °C and an important shoulder around 520 °C. Results of the quantitative analysis of the TPR curves are summarised in Table 2, where the molar ratios between hydrogen consumption and cobalt content are given. Previous studies [30] have shown that under the experimental conditions used, cobalt species are reduced to the zero-valent state. If only cobalt divalent species were reduced, the calculated values should be close to 1, considering the reduction reaction $CoO(s) + H_2(g) \rightarrow Co(s) + H_2O$. The values calculated are in good agreement with the presence exclusively of Co^{2+} species, in agreement with the vis–UV/DR spectra above mentioned. Although reduction of nitrate species would give rise to hydrogen consumption, they can only account for the weak peak around 350 °C, and we have previously shown [30] that carbonate species are decomposed before being reduced and that Al^{3+} species are not reduced under the experimental conditions used. Consequently, the over consumption of hydrogen may be only due to partial reduction of Zn^{2+} cations [31]. In some cases, the presence of several peaks in a TPR curve can be ascribed to a step-by-step reduction process, but in our case that would correspond to a reduction from Co^{2+} to Co^{1+} and then to Co^0. In such a case the areas of both peaks would be identical the same amount of hydrogen is needed in each of these two reduction steps. However, an approximate deconvolution of the two peaks indicates that the area of the first peak amounts ca. 25% of the total hydrogen consumption. Probably the presence of two peaks is due to the existence of cobalt cations with different access to the reducing molecules (i.e., hydrogen).

Table 2
S_{BET}, pore volume and quantitative results from TPR experiments of the LDH samples

Sample	S_{BET} ($m^2\ g^{-1}$)	V_p ($cm^3\ g^{-1}$)	H_2/Co[a]
CZA0	54	0.17	1.00
CZA10	52	0.15	0.99
CZA30	44	0.13	1.01
CZA60	41	0.11	1.06
CZA180	36	0.08	1.00
CZA300	34	0.08	1.09

[a] Rounded values.

The DTA and TG curves were recorded both in oxygen and nitrogen atmospheres. The influence of cobalt on the thermal properties of layered double hydroxides is well known, and consequently remarkable differences are found when the analyses are carried out in an inert or an oxidant atmosphere [32] (Fig. 2). The decomposition of hydrotalcite-like compounds usually proceeds in two steps such as water removal and hydroxyls and carbonates removal as CO_2 and H_2O, respectively. However, in compounds with cobalt the decomposition process is slightly different when performing the analyses in an oxidant atmosphere as a consequence of the oxidation and rapid formation of Co_3O_4. In order to evaluate the thermal stability of the synthesised compounds the analyses were carried out both in an oxidant and an inert atmosphere, by using N_2 and O_2 as gases during the thermal treatment. The thermal profiles are quite different, whereas for the former two peaks are clearly distinguished for the latter the second endothermic effect is overlapped to the water removal and it is displayed as a shoulder in some cases a small exothermic effect at ca. 400 °C is observed due to the $Co^{2+} \rightarrow Co^{3+}$ oxidation process [33]. In order to study the influence of the inclusion of Zn^{2+} cations in the structure and for sake of clarity, the DTA curve of a Co, Al sample was included in the graph.

It can be observed that under inert atmosphere conditions, CZA samples the second endothermic effect is shifted to lowers temperatures and its intensity is considerably reduced in comparison with the CA sample. Thus, it would appear that the presence of zinc cations decreases the stability of the hydrotalcite-like compounds, in fact in the DTA curve of Zn, Al compounds a single endothermic effect is recorded [34]. On the other hand, when the analyses are carried out in an oxygen atmosphere over free-Zn sample containing cobalt, a single endothermic effect was registered [35,36] whereas for ZnCoAl samples it seems that the inclusion of Zn^{2+} within the lamellar structure helps to stabilize the Co^{2+} delaying the oxidation process, since the peak is shifted towards higher temperatures and the shoulder is clearly observed.

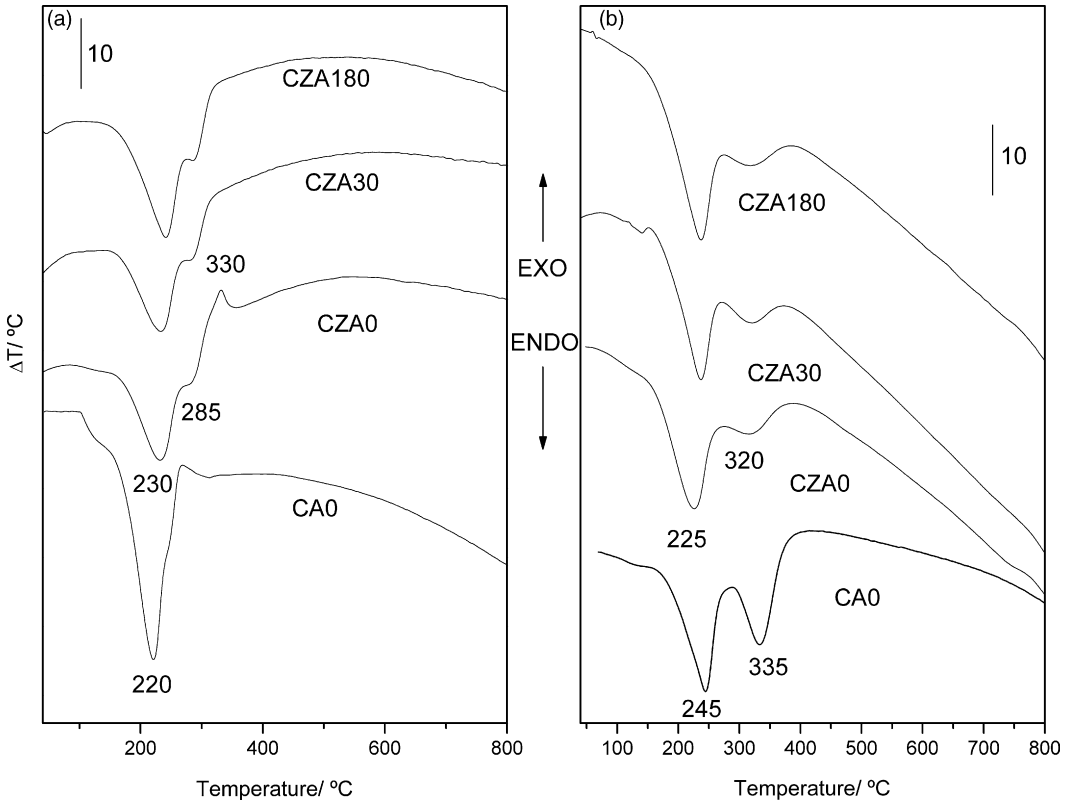

Fig. 2. Differential thermal analysis curves of some representative layered precursors, recorded in (a) oxygen and (b) nitrogen. The curves have been vertically displaced for clarity.

Finally, taking into account the effect of the microwave radiation on the thermal stability it can be seen that as the ageing treatment is prolonged (independent on the atmosphere) the first peak attributed to water removal (physisorbed and interlayer water) becomes more symmetric and narrower and it is shifted towards higher temperatures, suggesting that in these MW-treated samples the water molecules are more strongly bonded to the structure; narrowing of this peak suggests a more homogeneous interlamellar region with respect to the water molecules binding forces. On the other hand, when the analyses are performed in oxygen, the exothermic effect due to the oxidation of Co^{2+} to Co^{3+} is only observed for the non-treated sample, it would appear that the better ordering of the different species as a result of the MW treatment somewhat hinders oxidation of the Co^{2+} cations.

Thus we could conclude that the inclusion of Zn^{2+} cations influences the thermal stability of Co, Al-HTlcs and that an increase in the crystallinity of the samples, as a consequence of the MW treatment, also gives rise to thermal stabilisation of the solids.

The surface texture has been studied by nitrogen adsorption–desorption at −196 °C. The S_{BET} values, together with the total pore volumes, are summarized in Table 2. A progressive decrease in both magnitudes is observed as the irradiation time is extended, although in all cases rather large specific surface areas are measured. These results are in agreement with the PXRD data above mentioned. As the irradiation time is prolonged the particles become larger and less amorphous (leading to sharp diffraction maxima), where a partial, progressive cancellation of the pores and surface defects takes place, thus accounting for the smaller S_{BET} and V_p values. All the solids show type IIb isotherms [37], which are not modified after the MW ageing treatment. The shape of these curves indicates that all samples are either mesoporous or nonporous, without micropores. As the layered material has intrinsic micropores, corresponding to the low populated interlayer space, we should conclude, in agreement with previous results [38], that the nitrogen molecules are unable to penetrate in the interlayer space of the hydrotalcites. The absence of micropores is further confirmed by the *V–t* plots [39], which showed in all cases straight lines passing through the origin upon extrapolation. The BJH pore size distributions curves (not shown) show a main contribution of pores with a diameter close to ca. 4 nm, in addition to a broad and varied contribution (depending on the specific sample) by pores with diameters ranging from 2.5 to 10 nm.

3.2. Characterization of the calcined samples

The PXRD patterns of the calcined solids, Fig. 1b, show exclusively the diffraction peaks corresponding to a cubic spinel-like phase, indicating that the LDH structure has been completely destroyed. Single oxides CoO or ZnO are not either identified by PXRD in the solids, therefore it is concluded that the cobalt species are located in the spinel-like structure, although the presence of some amorphous material cannot be discounted entirely. These solids are less crystallised than the original LDHs, and the broadening of the peaks makes

Table 3
Cell parameters (a, in Å) particle size (D, in Å), S_{BET}, pore volume and quantitative results from TPR experiments for the calcined samples

Sample	a	D	S_{BET} ($m^2\ g^{-1}$)	V_p ($cm^3\ g^{-1}$)	H_2/Co[a]
CZA0c	7.32	100	67	0.20	1.56
CZA10c	7.33	95	59	0.15	
CZA30c	7.32	100	57	0.13	1.56
CZA60c	7.31	100	53	0.12	
CZA180c	7.33	110	49	0.11	1.58
CZA300c	7.33	115	48	0.11	

[a] Rounded values.

impossible to ascertain which particular spinel is formed, since there is hardly any difference between the spacings (and thereof the diffraction angles) of the spinels corresponding to the different metallic cations; the reflections can be due to several phases, such as Co_3O_4, $ZnCo_2O_4$, $ZnAl_2O_4$, $CoAl_2O_4$, or Co(Co, Al)O_4. However, it should be remembered the high tendency of Co^{3+} and Zn^{2+} to form a normal spinel-like structure, in which cobalt cations would occupy the octahedral sites; for this reason the most feasible structures existing after the calcination treatment could be $ZnCo_2O_4$ and Co(Co, Al)O_4 [40]. From the sharpness of the most intense diffraction peaks it seems that the crystallinity degrees are very close in all cases; a quantitative determination of the crystallite size, Table 3, indicates that the values are almost coincident (105 ± 10 Å) for all samples. The lattice parameter, determined from the position of the peak corresponding to diffraction by planes (3 1 1), is also almost coincident for all samples (Table 3).

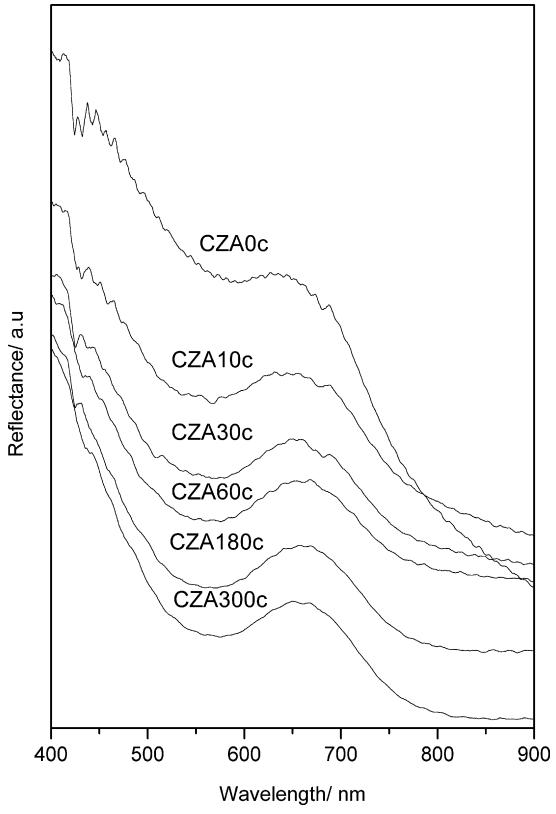

Fig. 3. Visible–ultraviolet/diffuse reflectance of the mixed oxides.

The vis–UV spectra for the calcined samples, Fig. 3, show an intense absorption between 400 and 700 nm; and a shoulder, which precise position depends on the particular sample, can be recorded at high wavelengths. The spectra, are very similar to that of a Co_3O_4 spinel phase; contained bands at 400 and 700 nm, which could be assigned to the transitions $^1A_{1g}(I) \rightarrow {}^1T_{2g}(I)$ and $^1A_{1g}(I) \rightarrow {}^1T_{1g}(I)$, respectively for a Co^{3+} in octahedral symmetry [28]. The absorption bands due to divalent cobalt in the spectra cannot be excluded, which should be registered at 515, 690 and 1300 nm, but the high absorption of the bands due to the trivalent species mask these bands.

The FT-IR spectra of the oxides showed the presence of the OH stretch at ca. 3400 cm^{-1} and the OH bending mode at ca.1635 cm^{-1} indicating that the surfaces were hydroxilated because the samples were exposed to the ambient after calcination and some water was adsorbed probably on the external surface of the samples during handling to record the spectra. The spectra also contained two strong absorption bands at 659 and 565 cm^{-1}, Fig. 4, which coincides with that reported in the literature for $ZnCo_2O_4$ spinel [41]. The former peak at 659 cm^{-1} is attributed to the stretching vibration mode of M–O for the tetrahedrally coordinated metal ions. The band at 565 cm^{-1} can be assigned to the octahedrally coordinated metal ions.

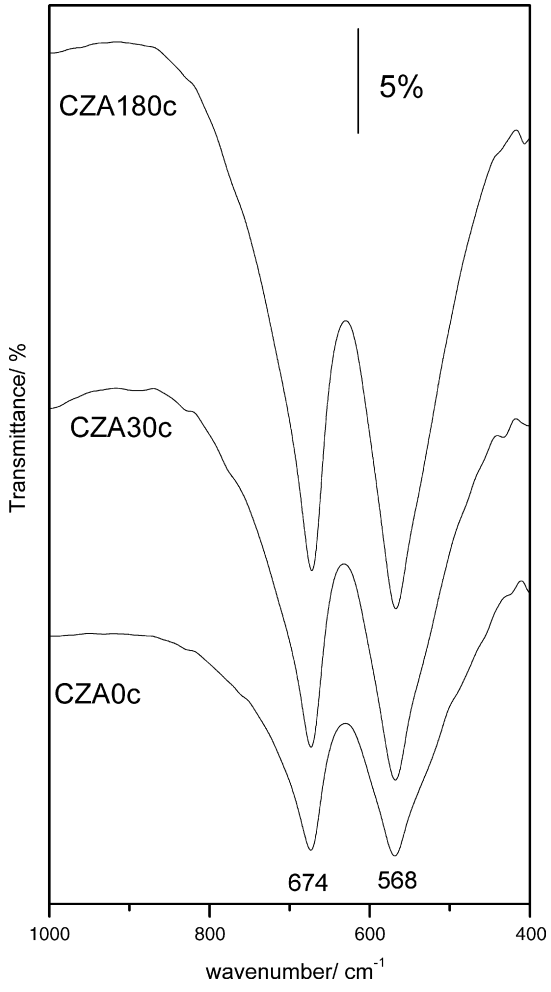

Fig. 4. FT-IR spectra of the some calcined samples. The curves have been vertically displaced for clarity.

The specific surface area values of the oxides are summarised in Table 3. They are 25–40% larger than those for the corresponding LDHs, and also a decrease is observed as the exposure time to MW of the original LDH is prolonged. The pore volumes are also ca. 20–30% larger than for the original LDHs. The N_2 isotherms, Fig. 5a, show different shapes depending on the particular solid. So, untreated sample CZA0c shows an isotherm similar to that of its LDH precursor and characteristic of nonporous or macroporous materials with an hysteresis loop due to slit shaped pores because of the agglomeration of the LDH platelets. For sample CZA10c, the process does not differ from that observed for sample CZA0c at low relative pressures; however, the slope raises at high relative pressures indicating an increased uptake of adsorbate due to adsorption in mesopores, which leads to multilayer formation until condensation takes place at a given pressure, giving rise thus to a sharp adsorption volume increase. The uptake is shifted towards lower relative pressures for the solids derived from the longer time MW-treated precursors. In addition, regarding the hysteresis loops of these isotherms, the shape is different before and after the plateau, suggesting the existence of two kinds of adsorption pores. Very narrow H3 hysteresis loops are found at high pressures, while at lower pressures the adsorption and desorption branches are not parallel, a behaviour characteristic of solids whose pore structures are complex and tend to be made up of interconnected networks of pores of different size and shape (where both pore size distribution and pore shape are not well defined) [37]. The BJH curves for porosity assessment, Fig. 5b, reveal significant modifications in the pore size depending on the ageing treatment the LDH precursors had been submitted to. Sample CZA0c shows a monomodal distribution curve with pores around 4 nm. However, the solids derived from the LDHs aged for long periods of time exhibit a bimodal distribution with pores around 3.5 and 7.5, the contribution of the latter ones being larger than that by the narrower pores.

The TPR profiles of representative calcined samples shown two H_2 consumption domains exist for all samples, at around 450 and 650 °C, pointing to the presence of two cobalt species [29] or species with different reducibility easiness. Results of a quantitative analysis of these curves is included in Table 3. While the second, intense maximum is recorded almost in the same temperature range as for the uncalcined solids (only shifted ca. 20–25 °C to lower temperatures), the first peak has shifted almost 100 °C to lower temperatures and now is clearly recorded as the result of, at least, two component peaks; actually, while for sample CZA30c both components seem to have the same intensity and the top part of the peak resembles a plateau, the absolute maximum is recorded at 385 °C for sample CZA0c, but at 450 °C for sample CZA180c. Consumption of hydrogen for the first peak is ca. 33% of total hydrogen consumption. In absolute terms, however, hydrogen consumption is too large to correspond to reduction of Co^{2+} cations (the expected H_2/Co ratio would be 1) or to Co^{2+} and Co^{3+} cations in the Co_3O_4 spinel (with an expected

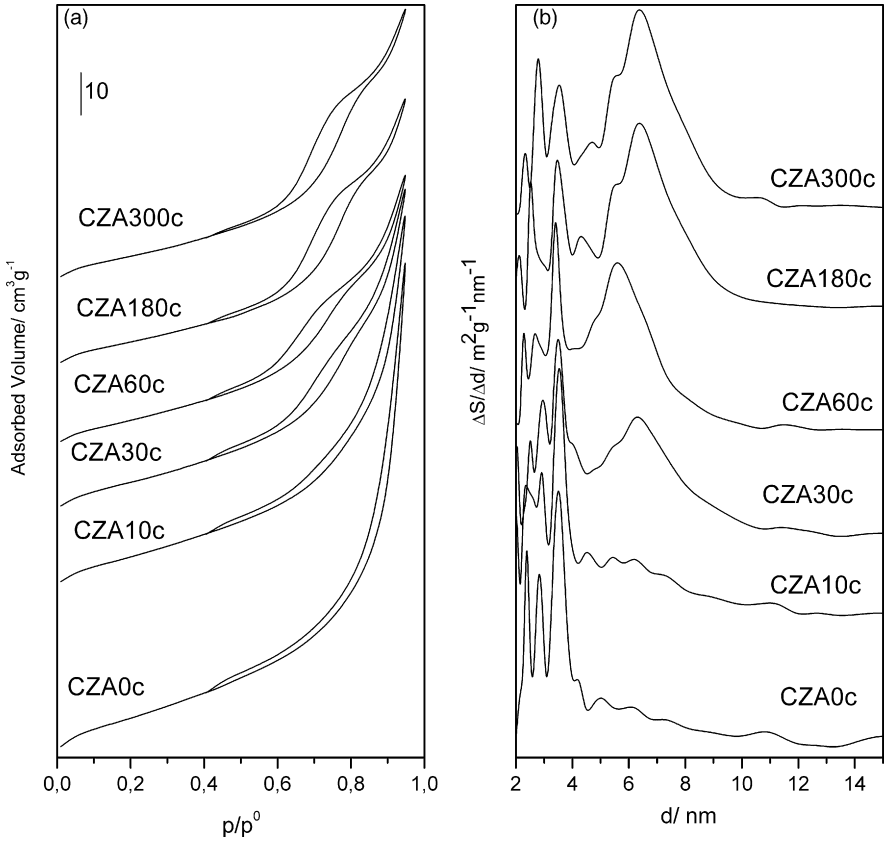

Fig. 5. N_2 adsorption/desorption isotherms (a) and BJH pore size distribution (b) for the calcined oxides. The patterns have been vertically displaced for clarity.

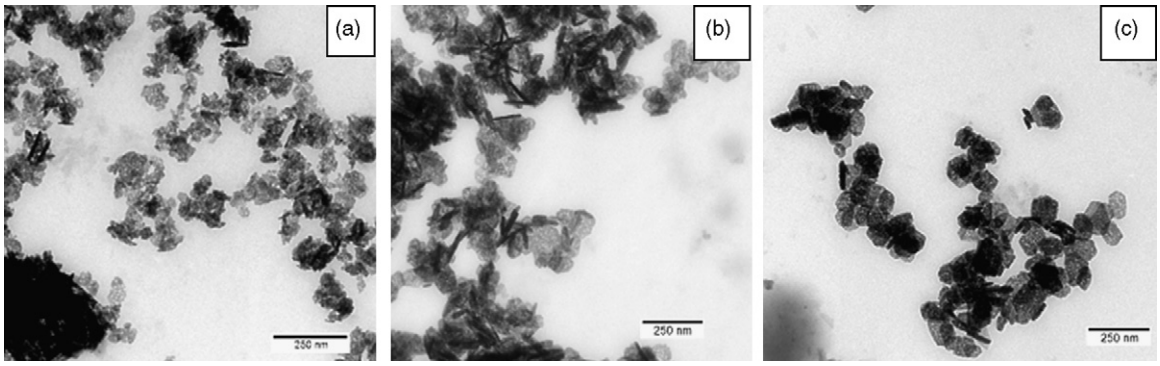

Fig. 6. Transmission electron micrographs of the calcined oxides (a) CZA0c, (b) CZA30c, and (c) CZA180.

H_2/Co ratio of 1.33). In our case, the value is close to that expected if all cobalt cations are in the 3+ state (expected value 1.5). The ratio between the intensities of both peaks is ca. 0.33:0.67, which could correspond to a step-by-step reduction ($Co^{3+} \rightarrow Co^{2+} \rightarrow Co^{0}$); unfortunately we could not confirm this supposition experimentally.

Regarding the particle shape, the TEM images for some representative calcined samples are displayed in Fig. 6. Significant differences in particles shape and size are observed by TEM, depending on the ageing treatment given to the precursor. Thin agglomerated particles are observed in sample CZA0c, while the MW-treated calcined samples keep well-defined hexagonal platelets, as previously observed in well-crystallised LDH.

4. Conclusions

Calcination of layered double hydroxides containing cobalt, previously aged under microwave irradiation, leads to mixed oxides containing Co^{3+} species with the spinel structure. Both the original layered precursors and the oxides prepared by calcination at moderate temperatures the crystallites are always in the nanodomain. Application of microwaves leads to an improvement in the crystallinity of the layered solids, an ordering on the interlayer species and a slight decrease in the specific surface area. Preliminary studies of catalytic activity for single wall carbon nanotubes formation have shown that the aged catalysts provide better activity and stability during decomposition of methane. Furthermore, the duration of microwave-hydrothermal treatment also produces a change in the kind of carbon nanofilaments produced. Inclusion of Zn^{2+} cations in the MW-treated samples influences the thermal stability of Co, Al-HTlcs and gives rise to an increase in their crystallinity.

Acknowledgments

Authors thank financial support from MCyT (Grants MAT2003-06605-C02-01 and MAT2006-10800-C02-01), Fundación Samuel Solorzano and JCyL (grant SA030/03), ERDF, CONCORDE and to Mr. A. Montero for his assistance in obtaining some of the experimental results. P.B. acknowledges a grant from JCyL.

References

[1] M. Wojciechowska, W. Przystajko, M. Zieliński, Catal. Today 119 (2007) 338.
[2] G. Fornasari, S. Gusi, F. Trifiró, A. Vaccari, Ind. Eng. Chem. Res. 26 (8) (1987).
[3] G. Fierro, G. Ferraris, R. Dragone, M. Lo Jacono, M. Faticanti, Catal. Today 116 (2006) 38.
[4] C. Otero Areán, M. Peñarroya Mentruit, A.J. López López, J.B. Parra, Phys. Eng. Aspects 180 (2001) 253.
[5] F. Cavani, F. Trifiró, A. Vaccari, Catal. Today 11 (1991) 173.
[6] V. Rives, Layered Double Hydroxides: Present and Future, Nova Science Publishers, New York, 2001.
[7] S. Velu, k. Suzuki, M.P. Kapoor, S. Tomura, F. Ohashi, T. Osaki, Chem. Mater. 12 (2000) 719.
[8] V. Rives, O. Prieto, A. Dubey, S. Kannan, J. Catal. 220 (2003) 161.
[9] Z.P. Xu, H.C. Zeng, Chem. Mater. 13 (2001) 4555.
[10] A. Vaccari, Catal. Today 41 (1998) 53.
[11] S.H. Yu, M. Yooshimura, Adv. Funct. Mater. 12 (2002) 9.
[12] F. Li, J. Liu, D.G. Evans, X. Duan, Chem. Mater. 16 (2004) 1597.
[13] S. Möhmel, I. Kurzawski, D. Uecker, D. Müller, W. Gebner, Cryst. Res. Technol. 37 (2002) 359.
[14] S. Kannan, R.V. Jasra, J. Mater. Chem. 10 (2000) 2311.
[15] M.J. Climent, A. Corma, S. Iborra, K. Epping, A. Velty, J. Catal. 225 (2004) 316.
[16] P. Benito, M. Herrero, F.M. Labajos, V. Rives, Mater. Sci. Forum. 514 (2006) 1241.
[17] E.T. Thostenson, T.-W. Chou, Composites A 30 (1999) 1055.
[18] W.T. Reichle, Solid State Ionics 22 (1986) 135.
[19] JCPDS, Joint Committee on Powder Diffraction Standards, International Centre fir Diffraction Data, Pennsylvania, U.S.A., 1977.
[20] P. Malet, J. Caballero, J. Chem. Soc., Faraday Trans. 84 (1998) 2369.
[21] V. Rives, Adsorpt. Sci. Technol. 8 (1991) 95.
[22] J.M. Fernández, C. Barriga, M.A. Ullibarri, F.M. Labajos, V. Rives, Chem. Mater. 9 (1997) 312.
[23] A.S. Bookin, V.A. Drits, Clays Clay Miner. 41 (1993) 551.
[24] F. Trifirò, A. Vaccari, O. Clause, Catal. Today 21 (1994) 185.
[25] F.M. Labajos, V. Rives, M.A. Ulibarri, J. Mater. Sci. 27 (1992) 1546.
[26] J.T. Kloprogge, R.L. Frost, in: V. Rives (Ed.), Layered Double Hydroxides: Present and Future, Nova Sci. Pub. Inc., New York, 2001, pp. 155–192.
[27] J.T. Kloprogge, The application of vibrational spectroscopy to clay minerals and layered double hydroxides, in: J.T. Kloprogge (Ed.), CMS Workshop Lectures, vol. 13, The Clay Mineral Society, Aurora, CO, (2005), pp. 203–238.
[28] D. Sutton, Espectros electrónicos de los complejos de los metales de transición, Ed. Reverté, 1975.
[29] S. Ribet, D. Tichit, B. Coq, B. Ducourant, F. Morato, J. Solid State Chem. 142 (1999) 382.
[30] V. Rives, M.A. Ulibarri, A. Montero, Appl. Clay Sci. 10 (1995) 83.
[31] C. Barriga, F. Kooli, V. Rives, M.A. Ulibarri, in: M.L. Occelli, H. Kessler (Eds.), Synthesis of Porous Materials, Marcel Dekker, Inc., New York, 1996, pp. 661–674.

[32] J. Pérez-Ramírez, J. Overeijnder, F. Kapteijn, J.A. Moulijn, Appl. Catal. B 23 (1999) 59.
[33] M.A. Ulibarri, J.M. Fernández, F.M. Labajos, V. Rives, Chem. Mater. 3 (1991) 626.
[34] J.L. Guimaraes, R. Marangoni, L.P. Ramos, F. Wypych, J. Colloid Interf. Sci. 227 (2000) 445.
[35] M. Herrero, P. Benito, F.M. Labajos, V. Rives, J. Solid State Chem. 180 (2007) 873.
[36] J. Pérez-Ramírez, G. Mul, F. Kapteijn, J.A. Moulijn, Mater. Res. Bull. 36 (2001) 1767.
[37] K.S.W. Sing, D.H. Everett, R.A.W. Haul, L. Moscou, R. Pierotti, J. Rouquerol, T. Sieminiewska, Pure Appl. Chem. 57 (1985) 603.
[38] V. Rives, R.L. Frost, in: V. Rives (Ed.), Layered Double Hydroxides: Present and Future, Nova Sci. Pub. Inc., New York, 2001, pp. 229–250.
[39] S. Lowell, J.E. Shields, Powder Surface Area and porosity, Chapman & Hall, Londres, 1984.
[40] T. Baird, K.C. Campbell, P.J. Holliman, R.W. Hoyle, D. Stirling, B.P. Williams, M. Morris, J. Mater. Chem. 7 (1997) 319.
[41] X. Wei, D. Chen, W. Tang, Mater. Chem. Phys. 103 (2007) 54.